1
2

Diversity of Pacific Meridional Mode and its distinct impacts on El Niño-Southern Oscillation

3 Jiuwei Zhao[1], Jong-Seong Kug[1*], Jae-Heung Park[1] and Soon-Il An[2]

4 [1]Division of Environmental Science and Engineering, Pohang University of Science &
5 Technology (POSTECH), Pohang, Korea

6 [2]Department of Atmospheric Sciences, Yonsei Univeristy, Seoul, Korea

7 *Corresponding author: Prof. Jong-Seong Kug
8   Division of Environmental Science and Engineering (DESE),
9   Pohang University of Science and Technology (POSTECH), Korea.
10   Email: jskug1@gmail.com

11

12 **Key points:**

13 • The Pacific Meridional Mode has strong spatial diversity that can be separated into two
14   groups

15 • These two types of the spring PMM have distinct impacts on ENSO events in the
16   following winter

17 • We suggest an optimal pattern of the spring PMM for ENSO prediction

18

19 **Abstract**

20 Numerous studies have demonstrated that the Pacific Meridional Mode (PMM) plays a vital role

21 in determining El Niño-Southern Oscillation (ENSO) events in the following winter season.

22 However, little attention has been given to significant differences among the spatial patterns of

23 the PMM. Here we show that the PMM exhibits a large diversity in spatial patterns, leading to

24 distinct impacts on ENSO. Based on objective clustering analysis, two distinct spatial patterns of

25 PMM are detected. Cluster 1 (C1) PMM exhibits a strong sea surface temperature dipole over the

26 subtropical eastern Pacific and mid-latitude central Pacific whereas cluster 2 (C2) features a

27 dipole over the subtropical eastern Pacific and equatorial cold tongue region. We find that the C1

28 PMM is strongly linked to ENSO events while the C2 PMM has no statistically significant

29 relations with following ENSO. This gives new implications for ENSO dynamics and predictions.

30 **Key words:** PMM diversity, cluster, ENSO

31
32

1 Introduction

The North Pacific Meridional Mode (PMM) is characterized by an anomalous meridional sea surface temperature (SST) gradient coupled with anomalous winds from a cold to warm flank over the eastern North Pacific (ENP; Amaya, 2019; Chiang & Vimont, 2004; Vimont et al., 2003). Previous studies (Chang et al., 2007; Yu & Kim, 2011) have summarized that spring PMM events can trigger the following El Niño-Southern Oscillation (ENSO); the PMM is thus considered a crucial precursor for the prediction of ENSO events.

Numerous works have focused on the origin of the PMM and its impact on ENSO, as well as understanding the interactions between them. A branch of the PMM SST warming off coastal California in spring can enhance subtropical convection over the ENP, which can in turn induce westerly anomalies. Wind anomalies associated with this region are further attributed to the warming and southwestward extension of SSTs in the following seasons *via* the wind-evaporation-SST (WES) mechanism (Xie & Philander, 1994) and thereby trigger El Niño events through positive feedbacks over the equatorial Pacific. A seasonal foot-printing mechanism (SFM) was proposed by Vimont et al. (2001, 2003) to explain the potential influence of the North Pacific Oscillation (NPO; Rogers, 1981) on ENSO events. The NPO can induce anomalous SSTs over the subtropical North Pacific by affecting latent heat fluxes. Previous studies (Kao & Yu, 2009; Yu et al., 2010) have argued that SST anomalies induced by the SFM resemble the pattern of the PMM SST. These two extratropical SST patterns have therefore been treated as key players in linking the extratropical Pacific to ENSO.

More recently, PMM has also been considered as a crucial factor to induce ENSO diversity (Yu et al., 2010, 2017; Yang et al., 2018). Stuecker (2018) found that the PMM and central Pacific (CP) ENSO can excite mutually, implying a positive feedback between these two phenomena. Yu & Fang (2018) recently proposed that the SFM could significantly contribute to

central Paicific ENSO events while the charge–discharge mechanism has a greater influence on conventional ENSO events. The SFM contributes to SST anomalies over the subtropical ENP while the charge–discharge mechanism modulates SST anomalies over the cold tongue (CT) region, where the SST anomalies of the PMM show significant varibility. The connection between these anomalies and both conventional and CP ENSO events also implies spatial differences in anomalous PMM SST patterns.

Although previous studies have documented possible physical processes of the PMM in exciting ENSO events, it has been seldom discussed how efficiently the PMM can induce ENSO events. Park et al. (2013) showed that only 5 positive events among 12 were linked to El Niño events in the following year and argued that the spatial pattern of the NPO might be a critical parameter for controlling the evolution of ENSO. We noted from their study that the PMM patterns shown are visibly different between the two groups. As shown in Figure 1a, we found that approximately 40% (13) of all PMM events (33) are strongly related to ENSO events. By further tracking these two groups of PMM events, we found that the main differences were concentrated on their anomalous SST patterns (Fig. 1d and 1f), which may lead to different roles in inducing ENSO events. Previous studies have shown the ubiquity of diversity in ENSO (Ashok et al., 2007; Kug et al., 2009; Yeh et al., 2009; Wang et al. 2019a) and the Madden Julian Oscillation (Wang et al. 2019b). The PMM could also exhibit diversity in its spatial patterns, which would further result in distinct behavior affecting the ENSO events.

Here, we propose a method to objectively delineate the diversity of the PMM and its impact on ENSO events. The reanalysis datasets and clustering method used to classify PMM events in this study are introduced in Section 2. The diversity of PMM and its impacts on ENSO are described in Section 3. A brief summary and discussion is presented in Section 4.

2 Data and Methodology

Extended Reconstructed SST version 5 (ERSST.v5; Huang et al., 2017) data were downloaded from the National Oceanic and Atmospheric Administration with a horizontal resolution of 2º for the 1951-2018 period. Atmospheric circulation data with a $2.5º \times 2.5º$ horizontal resolution, including sea level pressure (SLP) and winds at 850 hPa for the same period were downloaded from National Centers for Environmental Prediction/National Centers for Atmospheric Research reanalysis version I (NCEP/NCAR V1; Kalnay et al., 1996).

The raw PMM was download from the University of Wisconsin-Madison (http://www.aos.wisc.edu/~dvimont/MModes/RealTime/PMM.RAW.txt), which contains both interannual and interdecadal variabilities (Liu et al., 2019). A fast Fourier transform method is used to filter out decadal variability (> 10 years) from both the reanalysis data and the PMM index. We confirmed that the results of the cluster analysis were not significantly changed when applied to non-filtered data. To exclude the impact of previous ENSO events on the spring (February-May averaged; FMAM) PMM event, we linearly removed the previous November-December-January (NDJ) ENSO (Nino3.4; 5ºS-5ºN, 120ºW-170ºW) signal from the PMM time series as in Ashok et al. (2007). We also tested the removal of simultaneous ENSO signals, finding that the result was consistent (Fig. S1).

An objective K-Means clustering method (Wang et al., 2019a, b; Wilks, 2011) was used to classify diverse PMM patterns. Firstly, we linearly removed the previous NDJ Nino3.4 signal from FMAM SSTs. Secondly, 33 PMM events were selected based on a criterion of ± 0.7 standard deviation of the filtered FMAM PMM index and all negative PMM events were transformed to positive ones such that we were not required to separate positive and negative PMM events into two groups, allowing us instead to focus on pattern diversity. Thirdly, SSTs over a fixed domain (20ºS-40ºN, 150ºE-60ºW) were selected and fed into a clustering model

104   using squared Euclidean distance to measure the similarity between each cluster member and the

105   corresponding cluster centroid. The silhouette criterion, whose value varies from -1 to 1, was

106   utilized to assess the skill of cluster analysis. A high silhouette value implies that the member has

107   a high similarity with its own cluster but a lower similarity with its neighboring clusters

108   (Kaufman & Rousseeuw, 2009).

109   **3 Results**

110   Previous studies have documented a statistically significant correlation between the spring

111   PMM and the following winter ENSO index (Anderson, 2003, 2007; Larson & Kirtman, 2014).

112   Figure 1a shows the spring PMM and the following winter Nino3.4 indices with interdecadal

113   variability removed. The correlation is 0.28 for the period 1951-2018 and 0.45 for the period

114   1979-2018, both exceeding 95% confidence levels. The significant lag correlation indicates that

115   the PMM is probably a good predictor of ENSO events. However, we evaluated 33 PMM events

116   with amplitudes greater than 0.7 standard deviation and found that 13 cases (6 positive and 7

117   negative cases marked with green bars in Figure 1a) corresponded to respective ENSO events,

118   whereas the other 20 cases (10 positive and 10 negative in red bars) were not directly related to

119   ENSO (Fig. 1a). This indicates that some PMM events are strongly related to ENSO but others

120   did not lead to the triggering of ENSO, implying the PMM-ENSO relationship is diverse.

121   Furthermore, we studied composites of spring and winter SST anomalies for these 33 cases (Fig.

122   1b-1g). The spring PMM events show a clear tripole SST pattern with large anomalies centered

123   over the southern CT, ENP and central North Pacific regions (Fig. 1b), but the following ENSO

124   signal is weak (Fig. 1c).

125   To clarify the relationship between PMM and ENSO, we conducted a composite analysis

126   by dividing PMM events into two groups: the first group is strongly related to ENSO events (blue

127   bars) and the second is not (red bars; Fig. 1d-1g). An important feature shown is the significant

128   difference in spring PMM patterns between the two groups (Fig. 1d and 1f). When the positive

129   PMM precedes El Niño, the SST anomalies in spring show a clear dipole pattern in the northern

130   subtropical region but insignificant negative SST anomalies over the CT region (Fig. 1d). While

131   the PMM is not linked to ENSO development, the SST pattern shows an interhemispheric dipole

132   over the eastern Pacific. In addition, subtropical positive SST anomalies in Figure 1d extend to

133   the southwest as far as the equator over the CP, but negative SST anomalies are dominant over

134   the CT region in Figure 1f, mainly over the southeastern Pacific Ocean.

135   Abovementioned different SST patterns suggest potential spatial diversity in the PMM,

136   which could further lead to distinct impacts on ENSO events (Fig. 1e and 1g). To validate our

137   hypothesis and justify the corresponding analysis, a K-Means clustering method was utilized to

138   objectively classify 33 PMM events into 2 clusters. The composites of the PMM events for the

139   two clusters are shown in Figure 2, with different clusters displayed in the left and right panels.

140   Cluster 1 (C1) positive PMM events in Figure 2a are characterized by significant positive SST

141   anomalies elongated from the CP to the subtropical ENP and negative SST anomalies over the

142   subtropical CP region. C1 SST anomalies correspond to significant equatorial westerly anomalies

143   in the CP and easterly anomalies in the CT regions (Fig. 2a). Similarly, negative C1 events show

144   a strong negative SST anomaly extending from the CP to subtropical ENP, coupled with

145   significant equatorial easterly wind anomalies in the central-western Pacific, and a positive SST

146   anomaly in the subtropical North Pacific (Fig. 2b). However, the spatial pattern of cluster 2 (C2)

147   PMM events (Fig. 2d and 2f) is distinct from that of C1. C2 PMM events feature a hemispheric

148   dipole of SST anomalies over the southern tropical and northern subtropical eastern Pacific (Fig.

149   2d and 2f). Due to the development of strong SST anomalies over the CT region, easterly

150   anomalies are dominant over the whole equatorial Pacific during positive phases while westerly

151   anomalies during negative phases. These are clearly distinguished from their respective

152   anomalous convergent and divergent patterns in C1 events (Fig. 2a and 2b).

153   Based on the different spatial patterns of these two types of PMM events, we refer to C1 as the

154   western PMM (WPMM) and C2 as the eastern PMM (EPMM) events. The silhouette values of

155   C1 and C2 PMM events are shown in Figure 2c and 2f with positive and negative PMM cases

156   marked in red and blue, respectively. The silhouette values of C1 are, on average, higher than

157   those of C2, indicating that the C1 shows a higher degree of "similarity" and that the spatial

158   patterns of positive and negative WPMM events are more symmetric than the EPMM events. It is

159   worth noting that 5 El Niño events occurred in positive WPMM years where only one event

160   followed a positive EPMM phase. Moreover, only one La Niña event was involved in a positive

161   WPMM phase (Fig. S2a and Table S1) and no false alarms for El Niño events were observed

162   during our studying period, indicating that WPMM events are a better precursor for predicting

163   ENSO events.

164   Table S1 gives the details of ENSO events related to the PMM. Five of the seven positive C1

165   events were clearly linked to the occurrence of El Niño and four of the eight negative C1 events

166   were related to La Niña; each individual PMM case is shown in Figure S2. However, only one

167   positive EPMM event out of the nine cases studied was followed by an El Niño event, whereas

168   three of the nine negative EPMM events were followed by La Niña. It was also noted that the

169   positive EPMM event followed by an El Niño case corresponded to the only negative silhouette

170   value in C2 (Fig. 2f), meaning that this event was not a conventional EPMM event pattern.

171   Furthermore, 2 positive EPMM and 3 negative EPMM events were even followed by La Niña

172   and El Niño events, respectively, indicating false (or opposite) alarms. These results suggest that

173 relationships between PMM and ENSO are highly dependent on the pattern of the PMM.

174 Figure 3 shows the NDJ SST and 850 hPa wind anomalies corresponding to positive and

175 negative PMM events for two clusters. As expected from Table S1, the central-eastern Pacific is

176 covered by strong SST anomalies with prevailing westerly anomalies during the positive phase of

177 WPMM. The positive SST and westerly wind anomalies gradually developed from the CP with

178 strong off-equatorial signals during the developing phase (Fig. S3a). However, EPMM events do

179 not show any significant SST anomalies in the following winter (Fig. 3c and 3d), since strong

180 negative SST anomalies exist during May-June-July (Fig. S3c). Similarly, negative WPMM

181 events are followed by negative SST anomalies in the central and eastern Pacific with easterly

182 anomalies (Fig. S3b). It is also found that SST anomalies are more significant in the equatorial

183 CP. Yu and Fang (2018) previously suggested that PMM events are more closely related to the

184 development of CP SST anomalies than eastern Pacific SST anomalies, however, EPMM events

185 do not show a strong signal in the equatorial CP.

186 The strong linkage of WPMM to ENSO development can be explained by its pattern in

187 the equatorial western Pacific. As shown in Figure 3a, strong westerlies prevail in the western

188 Pacific. Since these westerlies are accompanied by positive equatorial CP SSTs, they can persist

189 and be intensified *via* strong air-sea interactions. The western Pacific westerlies induce

190 downwelling Kelvin waves, which play a role in recharging heat content in the central and

191 eastern Pacific (Kug et al. 2010). In addition, these low-frequency westerly anomalies provide a

192 preferable condition for easterly vertical shear of strong westerly wind events (Kug et al., 2009,

193 2010; Sooraj et al., 2009), a typical pattern of El Niño onset. Therefore, they evolve into a typical

194 El Niño pattern in the following summer and develop further until the end of the calendar year

195 (Fig. 3). However, positive SST anomalies resulting from the positive EPMM are confined to the

196 off-equatorial Pacific (Fig. 2d), which cannot trigger coupled equatorial patterns such as

197 equatorial westerlies and positive CP SST anomaly (Fig. 3c). Without the equatorial western

198 Pacific signals, El Niño tends not to develop. In addition, the prevailing negative SST anomalies

199 and their associated easterlies in the eastern Pacific may play a counteracting role in El Niño

200 development. Consequently, EPMM events are significantly related to El Niño development.

201   It is well known that the PMM is a useful predictor for ENSO, but PMM events are not

202 always followed by ENSO development, suggesting the existence of some false alarms. Thus far,

203 we showed that there is a preferable pattern of PMM for ENSO development. Our finding

204 suggests that false alarms from PMM information can be reduced if we considered the pattern

205 diversity of the PMM. Following previous methods (Kug et al., 2007; Zhu et al., 2015), we

206 attempted to reconstruct the PMM index based on the two types of spatial SST patterns and

207 comparison with the original PMM index. These new PMM indices depending on PMM diversity

208 are calculated by projecting the C1 and C2 SST patterns shown in Figure 2 into SST anomalies

209 each year (FMAM), and refer to WPMM and EPMM indices, respectively. The correlation

210 coefficient between the ENSO indices and the original PMM index is 0.28 (Fig. 4a); although this

211 is significant, it is difficult to use for prediction. Out of the 33 PMM events defined based on the

212 original PMM events, 13 cases resulted in ENSO development while another 6 PMM events (3

213 positive and 3 negative cases) were followed by the opposite phases of ENSO. Furthermore, the

214 last 14 PMM events were not linked to ENSO events. Using WPMM events, the correlation

215 increases significantly, reaching 0.64 between the WPMM and ENSO indices (Fig. 4b). We

216 found that WPMM captures 17 ENSO events among the 27 studied WPMM events (14 positive

217 and 13 negative cases) based on 0.7 standard deviation. In detail, 71.4% of positive WPMM

218 events (10 cases) eventually induce El Niño and 53.8% of negative PMM events (7 cases) lead to

219 La Niña, indicating that the hit rate is 63% on average, which is higher than the 39.4% based on

220 the original PMM index. Moreover, WPMM contains only 2 false alarms among the 27 events,

221 which is an improvement relative to the 6 false alarms in the original PMM events. Furthermore,

222 we also reconstructed the PMM index based on C2 SST patterns, finding that the correlation

223 between EPMM and ENSO is -0.22 (Fig. 4c). This indicates that EPMM cannot be used for

224 ENSO prediction.

225 **4 Conclusion and Discussion**

226 Most previous studies have emphasized that the PMM has a crucial role in triggering

227 ENSO events, however, it has seldom been noticed that the PMM is diverse. This diversity may

228 contribute to its variable impacts on ENSO. Based on the SST patterns, an objective clustering

229 method was used to classify PMM events. We found that PMM cases can be separated into two

230 groups. The WPMM is characterized by a dipole SST anomaly over the west part of ENP

231 whereas the EPMM dominates the CT and coastal SST anomalies in the ENP. Moreover, we

232 showed that approximately 60% of C1 PMM events (5 positive and 4 negative events among 15

233 C1 PMM cases) are significantly linked to ENSO events, while C2 PMM events are less notably

234 related to ENSO. To utilize our findings for ENSO prediction, we reconstructed WPMM and

235 EPMM indices and found that the WPMM index can accurately predict ENSO events with the

236 higher hit rate (63%) and with fewer false alarm than the original PMM index. The EPMM index

237 constructed based on C2 PMM SST patterns showed an insignificant negative relationship with

238 ENSO, implying that the EPMM SST pattern is not a good predictive framework for ENSO

239 events and requires further investigation.

240 Although we showed the PMM diversity and its distinct impacts on ENSO, it is not clear

241 what induced this diversity. Previous studies have documented that the NPO has different spatial

242 structures and that an eastward shift of the NPO may favor ENSO occurrence in the following

243 year while the classic NPO pattern with an elongated southern lobe is less related to ENSO

244 occurrence (Park et al. 2013; Sung et al., 2019; Yeh et al., 2018). We also found that the NDJ SLP

245 patterns preceding FMAM PMM are considerably different (Fig. S4). Clearly, WPMM events are

246 related to strong NPO events with a significant eastward shift (Fig. S4a and S4b), consistent with

247 Park et al (2013) and Yeh et al (2018). However, unlike previous studies, we found that EPMM

248 events are less linked to NPO events (Fig. S4c and S4d). Negative EPMM events are associated

249 with significantly negative SLP anomalies over North America but weak positive anomalies

250 south of 40ºN (Fig. S4d). In addition to the impact of NPO, it is also possible that PMM diversity

251 may be connected with SST variability in other basins. For example, some studies have

252 emphasized that the tropical Atlantic SST can modulate off-equatorial SST and wind variabilities

253 along the Pacific ITCZ (Ham et al., 2013; Ham & Kug, 2015; Park et al., 2018; 2019a,b), where

254 the action center of the PMM is located. Moreover, previous studies also found the decadal

255 variation of the PMM is related to the Pacific Decadal Oscillation (PDO; Newman et al., 2016).

256 In this study, however, the decadal variability of the PMM was screened out before the analyses.

257 The mechanism responsible for PMM diversity and its relationship with decadal modes should be

258 a focus of future research.

259

269
270

271   **References**

272   Amaya, D. J. (2019). The Pacific Meridional Mode and ENSO: a Review. *Current Climate*

273   *Change Reports*, *5*(4), 296–307. https://doi.org/10.1007/s40641-019-00142-x

274   Anderson, B. T. (2003). Tropical Pacific sea-surface temperatures and preceding sea level

275   pressure anomalies in the subtropical North Pacific. *Journal of Geophysical Research*,

276   *108*(D23), 4732. https://doi.org/10.1029/2003JD003805

277   Anderson, B. T. (2007). On the joint role of subtropical atmospheric variability and equatorial

278   subsurface heat content anomalies in initiating the onset of ENSO events. *Journal of*

279   *Climate*, *20*(8), 1593–1599. https://doi.org/10.1175/JCLI4075.1

280   Ashok, K., Behera, S. K., Rao, S. A., Weng, H., & Yamagata, T. (2007). El Niño Modoki and its

281   possible teleconnection. *Journal of Geophysical Research*, *112*(C11).

282   https://doi.org/10.1029/2006JC003798

283   Chang, P., Zhang, L., Saravanan, R., Vimont, D. J., Chiang, J. C. H., Ji, L., et al. (2007). Pacific

284   meridional mode and El Niño-Southern Oscillation. *Geophysical Research Letters*, *34*(16).

285   https://doi.org/10.1029/2007GL030302

286   Chiang, J. C. H., & Vimont, D. J. (2004). Analogous Pacific and Atlantic Meridional Modes of

287   tropical atmosphere–ocean variability. *Journal of Climate*, *17*(21), 4143–4158.

288   https://doi.org/10.1175/JCLI4953.1

289   Ham, Y.-G., & Kug, J.-S. (2015). Role of north tropical Atlantic SST on the ENSO simulated

290   using CMIP3 and CMIP5 models. *Climate Dynamics*, *45*(11–12), 3103–3117.

291   https://doi.org/10.1007/s00382-015-2527-z

292   Ham, Y.-G., Kug, J.-S., Park, J.-Y., & Jin, F.-F. (2013). Sea surface temperature in the north

293   tropical Atlantic as a trigger for El Niño/Southern Oscillation events. *Nature Geoscience*,

294   *6*(2), 112–116. https://doi.org/10.1038/ngeo1686

295   Huang, B., Thorne, P. W., Banzon, V. F., Boyer, T., Chepurin, G., Lawrimore, J. H., et al. (2017).

296   Extended reconstructed sea surface temperature, Version 5 (ERSSTv5): Upgrades,

297   validations, and intercomparisons. *Journal of Climate*, *30*(20), 8179–8205.

298   https://doi.org/10.1175/JCLI-D-16-0836.1

299   Kalnay, E., Kanamitsu, M., Kistler, R., Collins, W., Deaven, D., Gandin, L., et al. (1996). The

300   NCEP/NCAR 40-year reanalysis project. *Bulletin of the American Meteorological Society*,

301   *77*(3), 437–471. https://doi.org/10.1175/1520-0477(1996)077<0437:TNYRP>2.0.CO;2

302   Kao, H.-Y., & Yu, J.-Y. (2009). Contrasting Eastern-Pacific and Central-Pacific Types of ENSO.

303   *Journal of Climate*, *22*(3), 615–632. https://doi.org/10.1175/2008JCLI2309.1

304   Kaufman, L., & Rousseeuw, P. J. (2009). *Finding groups in data: An introduction to cluster*

305   *analysis*. New York, NY: John Wiley & Sons. Retrieved from http://nbn-

306   resolving.de/urn:nbn:de:101:1-2014122810037

307   Kug, J.-S., Jin, F.-F., & An, S.-I. (2009). Two types of El Niño events: Cold tongue El Niño and

308   warm pool El Niño. *Journal of Climate*, *22*(6), 1499–1515.

309   https://doi.org/10.1175/2008JCLI2624.1

310   Kug, J.-S., Sooraj, K.-P., Li, T., & Jin, F.-F. (2010). Precursors of the El Niño/La Niña onset and

311   their interrelationship. *Journal of Geophysical Research*, *115*(D5), D05106.

312   https://doi.org/10.1029/2009JD012861

313   Kug, J.-S., Lee, J.-Y., & Kang, I.-S. (2007). Global sea surface temperature prediction using a

314   multimodel ensemble. *Monthly Weather Review*, *135*(9), 3239–3247.

315   https://doi.org/10.1175/MWR3458.1

316   Larson, S. M., & Kirtman, B. P. (2014). The Pacific Meridional Mode as an ENSO precursor and

317   predictor in the North American multimodel ensemble. *Journal of Climate*, *27*(18), 7018–

318   7032. https://doi.org/10.1175/JCLI-D-14-00055.1

319   Liu, C., Zhang, W., Stuecker, M. F., & Jin, F. (2019). Pacific Meridional Mode-Western North

320   Pacific tropical cyclone linkage explained by tropical Pacific quasi-decadal variability.

321   Geophysical Research Letters, 46(22), 13346–13354.

322   https://doi.org/10.1029/2019GL085340

323   Newman, M., Alexander, M. A., Ault, T. R., Cobb, K. M., Deser, C., Di Lorenzo, E., et al. (2016).

324   The Pacific Decadal Oscillation, revisited. *Journal of Climate*, *29*(12), 4399–4427.

325   https://doi.org/10.1175/JCLI-D-15-0508.1

326   Park, J.-H., Kug, J.-S., Li, T., & Behera, S. K. (2018). Predicting El Niño beyond 1-year lead:

327   Effect of the Western Hemisphere Warm Pool. *Scientific Reports*, *8*(1), 14957.

328   https://doi.org/10.1038/s41598-018-33191-7

329   Park, J.-H., Li, T., Yeh, S.-W., & Kim, H. (2019a). Effect of recent Atlantic warming in

330   strengthening Atlantic–Pacific teleconnection on interannual timescale via enhanced

331   connection with the Pacific Meridional Mode. *Climate Dynamics*, *53*(1–2), 371–387.

332   https://doi.org/10.1007/s00382-018-4591-7

333   Park, J.-H., Kug, J.-S., An, S.-I., & Li, T. (2019b). Role of the western hemisphere warm pool in

334   climate variability over the western North Pacific. *Climate Dynamics*.

335   https://doi.org/10.1007/s00382-019-04652-0

336   Park, J.-Y., Yeh, S.-W., Kug, J.-S., & Yoon, J. (2013). Favorable connections between seasonal

337   footprinting mechanism and El Niño. *Climate Dynamics*, *40*(5–6), 1169–1181.

338   https://doi.org/10.1007/s00382-012-1477-y

339   Rogers, J. C. (1981). The North Pacific Oscillation. *Journal of Climatology*, *1*(1), 39–57.

340   https://doi.org/10.1002/joc.3370010106

341   Sooraj, K. P., Kim, D., Kug, J.-S., Yeh, S.-W., Jin, F.-F., & Kang, I.-S. (2009). Effects of the

342   low-frequency zonal wind variation on the high frequency atmospheric variability over

343   the tropics. *Climate Dynamics*, *33*(4), 495–507. https://doi.org/10.1007/s00382-008-0483-

344   6

345   Stuecker, M. F. (2018). Revisiting the Pacific Meridional Mode. *Scientific Reports*, *8*(1), 3216.

346   https://doi.org/10.1038/s41598-018-21537-0

347   Sung, M.-K., Jang, H.-Y., Kim, B.-M., Yeh, S.-W., Choi, Y.-S., & Yoo, C. (2019). Tropical

348   influence on the North Pacific Oscillation drives winter extremes in North America.

349   *Nature Climate Change*, *9*(5), 413–418. https://doi.org/10.1038/s41558-019-0461-5

350   Vimont, D. J., Battisti, D. S., & Hirst, A. C. (2001). Footprinting: A seasonal connection between

351   the tropics and mid-latitudes. *Geophysical Research Letters*, *28*(20), 3923–3926.

352   https://doi.org/10.1029/2001GL013435

353   Vimont, D. J., Wallace, J. M., & Battisti, D. S. (2003). The seasonal footprinting mechanism in

354   the Pacific: Implications for ENSO. *Journal of Climate*, *16*(16), 2653–2667.

355   Wang, B., Luo, X., Yang, Y.-M., Sun, W., Cane, M. A., Cai, W., et al. (2019a). Historical change

356   of El Niño properties sheds light on future changes of extreme El Niño. *Proceedings of*

357   *the National Academy of Sciences*, *116*(45), 22512–22517.

358   https://doi.org/10.1073/pnas.1911130116

359   Wang, B., Chen, G., & Liu, F. (2019b). Diversity of the Madden-Julian Oscillation. *Science*

360   *Advances*, *5*(7), eaax0220. https://doi.org/10.1126/sciadv.aax0220

361   Wilks, D. S. (2011). *Statistical Methods in the Atmospheric Sciences*.

362   Xie, S.-P., & Philander, S. G. H. (1994). A coupled ocean-atmosphere model of relevance to the

363   ITCZ in the eastern Pacific. *Tellus A: Dynamic Meteorology and Oceanography*, *46*(4),

364   340–350. https://doi.org/10.3402/tellusa.v46i4.15484

365   Yang, S., Li, Z., Yu, J.-Y., Hu, X., Dong, W., & He, S. (2018). El Niño–Southern Oscillation and

366   its impact in the changing climate. *National Science Review*, *5*(6), 840–857.

367   https://doi.org/10.1093/nsr/nwy046

368   Yeh, S.-W., Kug, J.-S., Dewitte, B., Kwon, M.-H., Kirtman, B. P., & Jin, F.-F. (2009). El Niño in

369   a changing climate. *Nature*, *461*(7263), 511–514. https://doi.org/10.1038/nature08316

370   Yeh, S.-W., Yi, D.-W., Sung, M.-K., & Kim, Y. H. (2018). An eastward shift of the North Pacific

371   Oscillation after the mid-1990s and its relationship with ENSO. *Geophysical Research*

372   *Letters*, *45*(13), 6654–6660. https://doi.org/10.1029/2018GL078671

373   Yu, J.-Y., & Fang, S.-W. (2018). The distinct contributions of the seasonal footprinting and

374   charged-discharged mechanisms to ENSO complexity. *Geophysical Research Letters*,

375   *45*(13), 6611–6618. https://doi.org/10.1029/2018GL077664

376   Yu, J.-Y., & Kim, S. T. (2011). Relationships between extratropical sea level pressure variations

377   and the Central Pacific and Eastern Pacific types of ENSO. *Journal of Climate*, *24*(3),

378   708–720. https://doi.org/10.1175/2010JCLI3688.1

379   Yu, J.-Y., Kao, H.-Y., & Lee, T. (2010). Subtropics-related interannual sea surface temperature

380   variability in the Central Equatorial Pacific. *Journal of Climate*, *23*(11), 2869–2884.

381   https://doi.org/10.1175/2010JCLI3171.1

382   Yu, J.-Y., Wang, X., Yang, S., Paek, H., & Chen, M. (2017). The changing El Niño-Southern

383   Oscillation and associated climate extremes. In S.-Y. S. Wang, J.-H. Yoon, C. C. Funk, &

384   R. R. Gillies (Eds.), *Geophysical Monograph Series* (pp. 1–38). Hoboken, NJ, USA: John

385   Wiley & Sons, Inc. https://doi.org/10.1002/9781119068020.ch1

386 Zhu, Z., Li, T., Hsu, P., & He, J. (2015). A spatial–temporal projection model for extended-range

387   forecast in the tropics. Climate Dynamics, 45(3–4), 1085–1098.

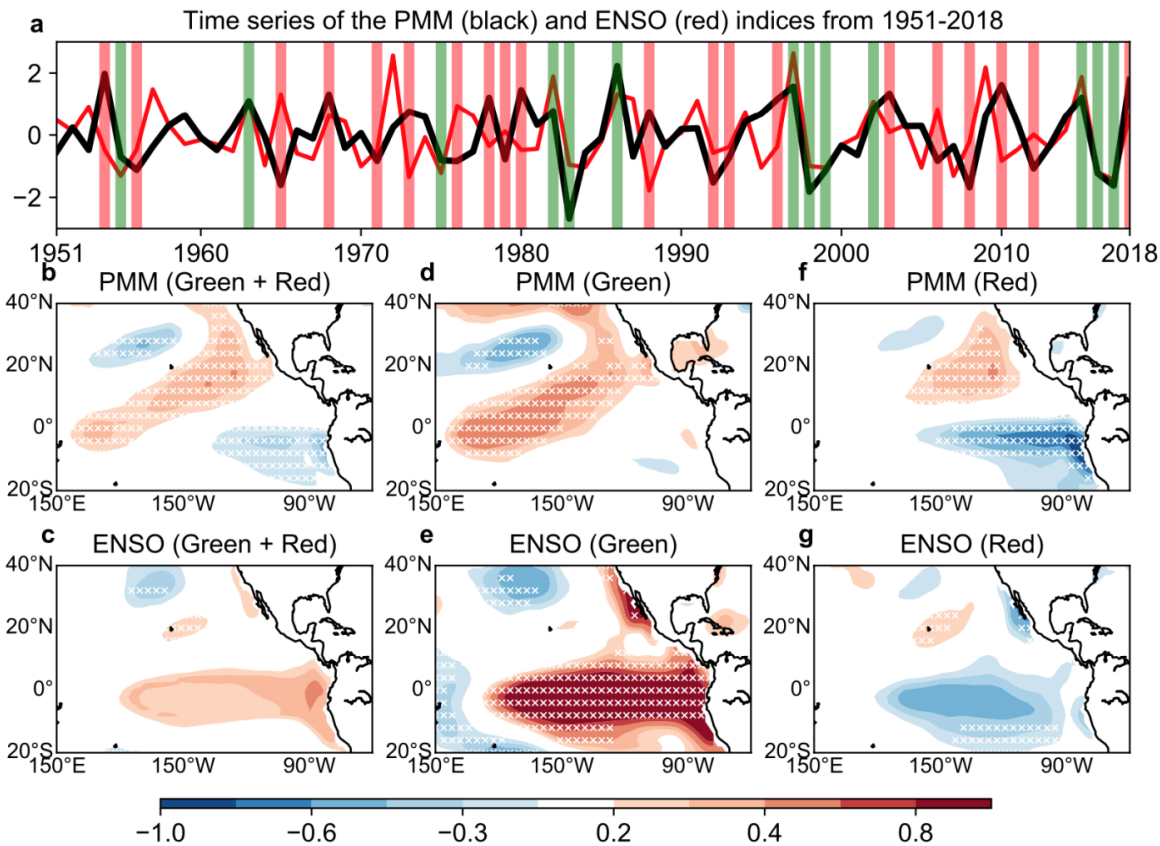388   https://doi.org/10.1007/s00382-014-2353-8

389

390

Figures:

Figure 1. Time series (a) of the PMM and ENSO indices from 1951-2018 and the spring (FMAM; b, d and f) and winter (NDJ; c, e and g) SST anomalies between positive and negative PMM years. (a) Normalized PMM (black line) and following NDJ averaged Niño3.4 (red line) indices for the period 1951-2018. Green and red bars indicate PMM events larger than ±0.7 standard deviation. Green bars represent the 13 (6 positive and 7 negative) PMM events associated with ENSO occurrence while red bars represent the other 20 (10 positive and 10 negative) PMM events (i.e., a total of 33 PMM events). (b) the composite of SST anomalies from 16 positive and 17 negative PMM events; (c) corresponding NDJ SST anomalies based on 33 PMM events; (d) composite of SST anomalies of 13 PMM events shown as green bars; (e) composite of NDJ SST anomalies based on the 13 PMM years represented by green bars; (f) same as (d) but for the 20 PMM events indicated by red bars; (g) same as (e) but for the 20 PMM years shown as red bars. White crosses represent areas of SST above 95% significance level.
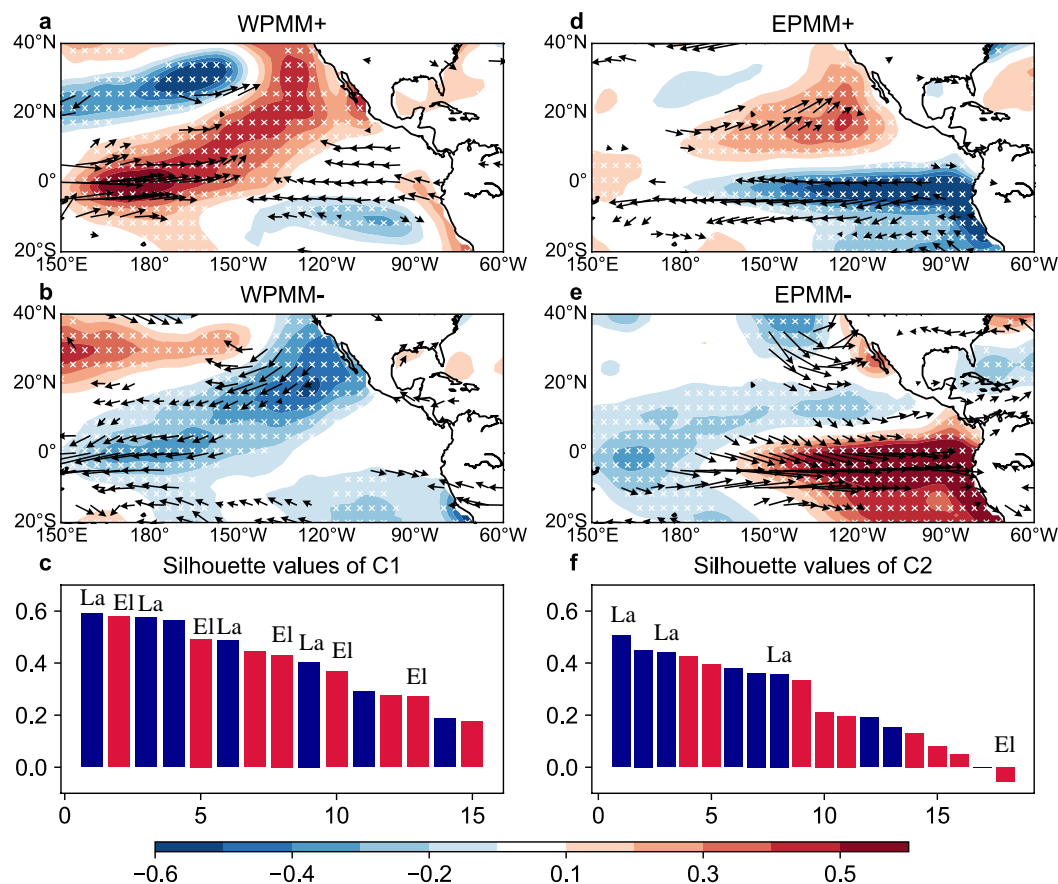
Figure 2. Two clusters of PMM events and silhouette values of each event. Cluster 1 (C1; left panel) (a) positive and (b) negative PMM events; cluster 2 (C2; right panel) (c) positive and (d) negative PMM events; silhouette values for (e) C1 and (f) C2 PMM events. White crosses in a, b, d and e represent areas of anomalous SST fields above 90% confidence level based on a two-tailed t test; black arrows indicate the composite of 850 hPa winds (m/s) above 90% confidence level. Red (blue) bars in (c) and (f) represent the positive (negative) PMM events, respectively. "El" and "La" marked above the bars in (c) and (f) indicate that El Niño or La Niña events occurred during the respective positive and negative PMM phases.
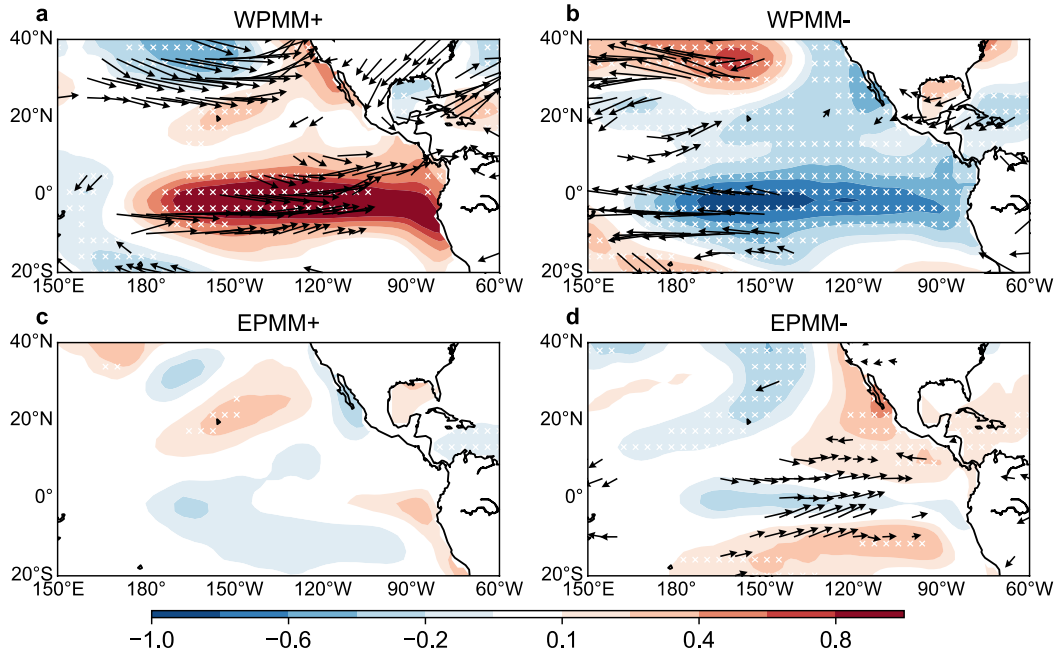
Figure 3. Composites of NDJ averaged SST anomalies and wind anomalies at 850hPa based on different types of PMM years. (a) Composite NDJ SST anomalies during C1 positive PMM years; (b) same as (a) but for C1 negative PMM years; (c) same as (a) but for C2 positive PMM years; and (d) same as (b) but for negative C2 PMM years. White crosses and black arrows indicate area above 90% confidence level.
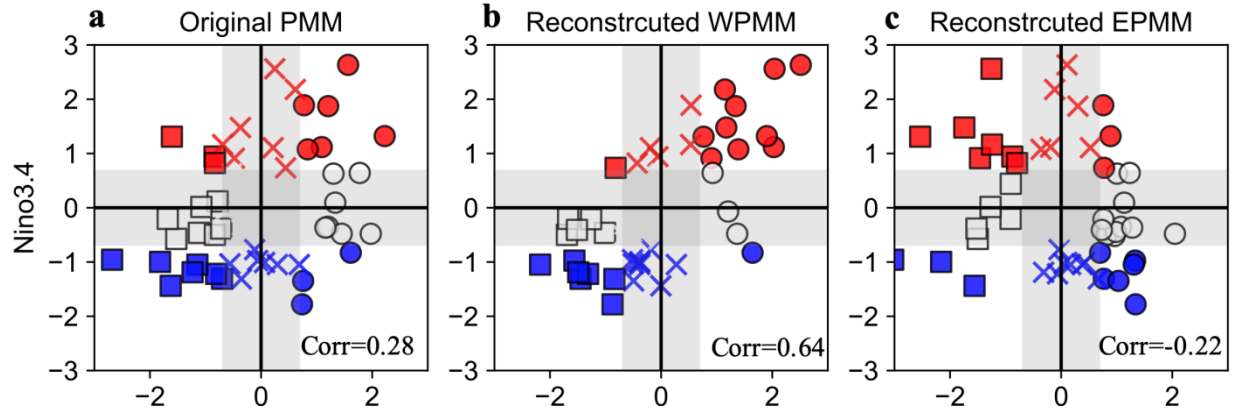
425

Figure 4. **Scatter diagrams of ENSO index and original (reconstructed) PMM index based on C1 and C2 spatial patterns for the period 1951-2018.** (a) Scatter plot of ENSO and original PMM indices; (b) scatter plot of ENSO index and WPMM index reconstructed based on the C1 SST pattern; and (c) scatter plot of ENSO index and EPMM index reconstructed based on the C2 SST pattern. Significant El Niño and La Niña events are colored red and blue, respectively. Significant positive and negative PMM events are marked by circles and rectangles, respectively.